On the Comprehensive Stability Analysis of Axially Loaded Bistable and Tristable Metastructures

E.G. Karpov*, D. Ozevin, M. Mahamid, and L.A. Danso

Department Civil & Materials Engineering, University of Illinois, Chicago, IL 60607, U.S.A.

*Corresponding author, email: ekarpov@uic.edu

Abstract: Approaches to systematic analysis of essentially nonlinear structures with multistable responses, controlled buckling and snapping behavior have received much attention recently in the context of mechanical metamaterials design. A snapping bistable element is generally a highly efficient damper, performing well even at very low forcing frequencies. In this paper, we transfer basic tools of the metamaterials analysis to macroscopic systems relevant to civil and mechanical engineering applications. Such systems are comprised of only several bistable elements. Followed by analysis of a single snapping bistable axial (two-force) element, we consider a combination of two elements with antisymmetric properties and demonstrate a robust *tristable* performance of the resultant structure in low-frequency or quasistatic tension-compression loading cycles. The tristability provides an overall response that is symmetric for tension and compression, which makes it interesting for applications in machinery and large-scale seismic structures.

1. Introduction

Materials with macroscopic internal structure offer novel opportunities in nonlinear acoustics [1-3], phononics [4-6] and exotic mechanical properties enabling futuristic engineering applications. Some interesting mechanical properties that have been realized includes negative Poisson's ratio [7-10], superelastic responses [11-14], negative compressibility [15-17], negative extensibility [18-20], reverse Saint-Venant's edge effect [21-24], strain energy control and redirection [23-24]. Also, internal structure design could provide materials with negative effective elastic moduli [25-28] and reverse thermal properties [29-33]. Inspired by earlier advances in multistable mechanical metamaterials [15-20], snapping thermomechanical metamaterials can demonstrate negative thermal expansion in a broad range of temperature and system parameters [34]. Multistability in dynamical systems also reveals promises for highly efficient energy harvesting, nonlinear resonances, switching waves, and nonreciprocal wave propagation [35-46].

Approaches to systematic analysis of essentially nonlinear structures with bistabilities, controlled buckling and snapping behavior have been discussed recently by Karpov and co-authors [11,19-20,34] in the context of mechanical metamaterials design. Mechanical *bistability* is defined as availability of two stable equilibrium configurations in the structure in response to the same loading conditions. These structures were intended as repetitive unit cells in multistable mechanical metamaterials. In this paper, we transfer basic tools and concepts of this analysis to macroscopic systems relevant to civil and mechanical engineering applications. While metamaterials usually contain a great number of bistable elements, resulting in an averaged performance, interesting large-scale applications may employ only one or several combined bistable elements for an unusual desired behavior.

Global buckling of diagonal brace elements in concentrically braced building frames has been traditionally designated as a viable energy-dissipation mechanism in structural engineering. A major concern with such mechanism is the premature fracture of the brace due to combined global and local buckling in the brace when subjected to cyclic loadings during an earthquake ground motion [47]. In addition, substantial difference of tension and compression strengths of the brace imposes significant demand on brace-intersected beams and beam-to-column connections. A popular solution to overcome premature brace fracture and to acquire stable cyclic response and significant energy absorption capability is to control global and local buckling of braces. Attempts to address these concerns resulted in various types of all-steel buckling-restrained brace (BRB). Here, the enhance performance gave rise to unnecessarily complex [48-51] all-steel BRB designs with closely spaced bolted or welded attachments [52] as well as sections built up by combining multiple structural shapes, described in the review [53], and some of the newly proposed option such as the three-segment steel brace [54]. Additionally, several self-centering energy dissipating elements has been proposed [55-64] that can be efficient in dissipating the energy when used in seismic braced frames but some require extensive detailing and others would also require pretensioned components. Thus, there remains a need for simple, practical and cost-effective solutions, suitable for existing connection types, enhancing fracture life of the braces and overall seismic performance of the concentrically braced frames without altering the current habits in the design and construction practice.

Advantages of the multistable axial members, or *"metabrace"* elements, discussed here is the absence of pretensioned elements, which may have durability issues during the structure's life span. These metabraces have a symmetric hysteresis at quasi-static loading, while the self-centering elements with pretensioned element can have hysteresis only in dynamical cycles with large damping, similar to a usual spring-mass damper. The tristable metabrace also has an internal degree of freedom to further enhance energy dissipation in slow load cycles through a state transition event. Additionally, tunability of the metabraces seems to be higher, which can even be made superplastic if needed.

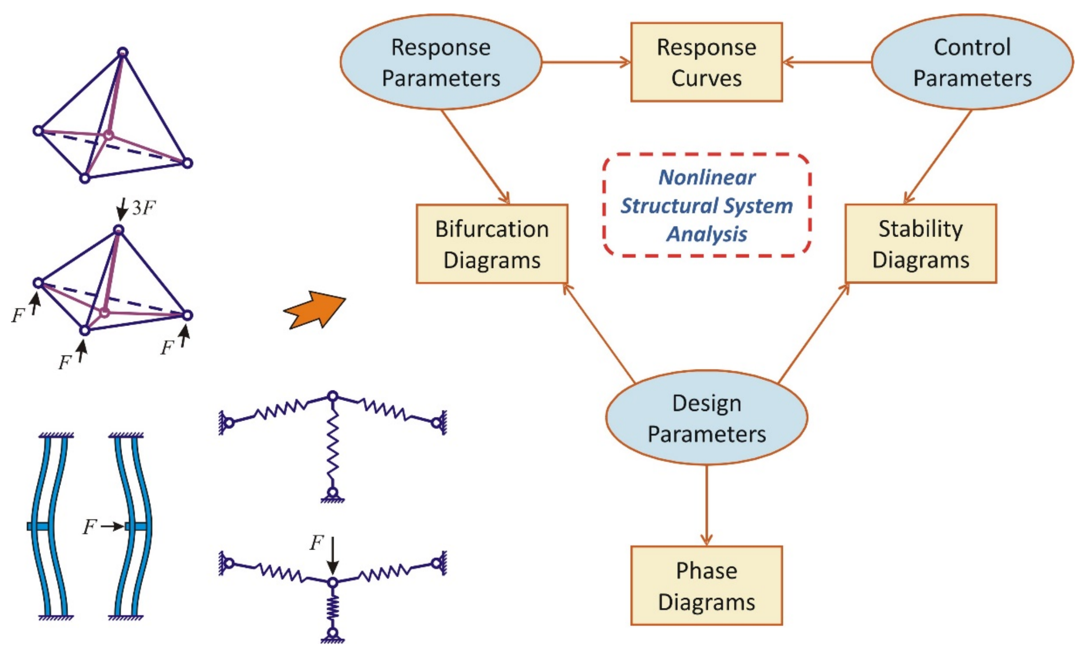

Fig.1: Examples of bistable structural units, and their comprehensive analysis approach.

Following the analysis of a single bistable axial (two-force) element, in this paper, we consider a combination of two elements with antisymmetric properties and demonstrate a robust *tristable* performance of the resultant structure in tension-compression loading cycles. The structure can be fabricated as an axial (two-force) member, a bar, or a structural brace to replace the corresponding axial element in steel building frames and bridges. State 1 of this elements is found around its relaxed configuration, a transition to State 2 occurs in tension, and to State 3 in compression. When the axial load is removed, the structure may or may not return to State 1, depending on the design; the details will follow. Tension-compression cycles are typical in various scenarios of seismic impact, while the bistable element is generally a highly promising damper, performing well even at very slow forcing frequencies [18]. In this paper, we will see that a combination of two bistable antisymmetric elements provides an overall response that is symmetric for tension and compression, due to the tristability, which makes it interesting for the large-scale structural applications.

For a systematic discussion, we utilize the logic summarized in the Figure 1 diagram. Similar to the study of metamaterials [11,19-20,34], we divide all the relevant physical parameters into three groups: (i) *system/design parameters* (describe unit cell geometry and material properties of basic structural elements), (ii) *control parameters* (describe external stimuli, such as mechanical or thermal loads), and (iii) *state parameters* or *behavior variables* (vary with external loads and describe state of deformation or thermal strain in response to that load). Theoretical, numerical or experimental relationships between the state parameters and control parameters may demonstrate interesting *physical behaviors or properties*, such as bistability, negative elastic moduli, or negative thermal expansion.

Furthermore, we refer to the diagrams mapping all possible types of physical behavior in terms of design parameters as *phase diagrams* [11,19-20,34]. Maps linking important design parameters with critical values of control parameters, such as those at the onset of phase transitions, are *stability diagrams* [11,19-20,34,65]. Plots of responses versus design parameters at fixed control parameters give *bifurcation diagrams*, and maps showing sample responses to external stimuli for given system parameters will be called *response curves*. The goal of this mapping is to provide relationships between desired interesting behaviors and the corresponding system parameters that should be used in practical designs to enable those behaviors. This systematic analysis can minimize or fully eliminate the trial and error effort, which otherwise is inevitable in the design of highly nonlinear structural systems.

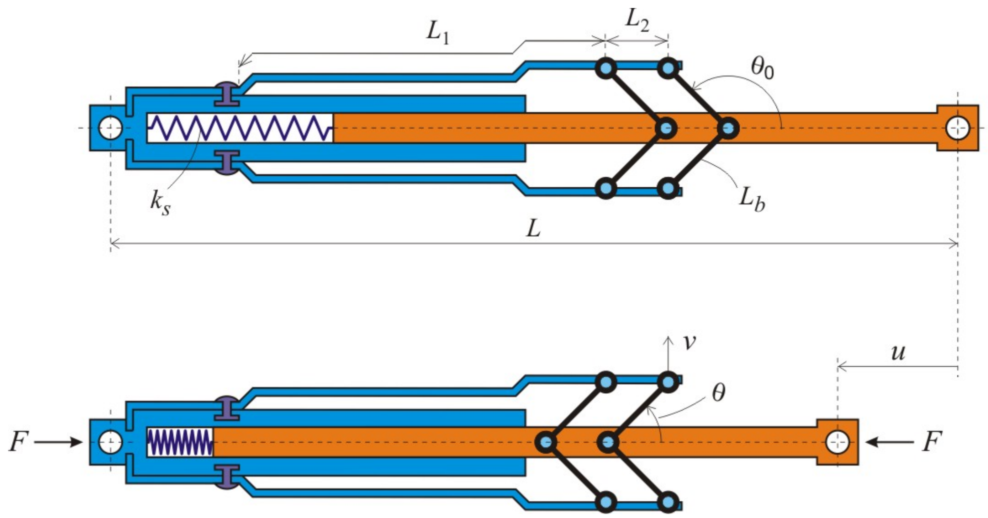

Fig.2: Bistable axial bar element: θ is inclination angle of the rigid hinged bars in a state of equilibrium for the external load F; u is horizontal displacement if the middle slider, v is vertical displacement of the flappers; L_b is length of the hinged bars; k_s is axial stiffness of the encapsulated spring; distances L_1 and L_2 and bending rigidity (EI) of the flappers determine its bending stiffness, $k_b = 12EI(3L_1 + L_2)/L_1^3(3L_1 + 4L_2)$; and θ_0 is initial of angle of the hinged bars, prior to loading.

2. Dimensionless Form of the Total Potential Energy

Various bistable unit cells were discussed in [11-12,19-20,34] in the context of periodic mechanical metamaterials. On the contrary, a bistable element to replace the usual bars, braces and other two-force members relevant to the structural engineering practice should have a slender design, as that in Figure 2. Thus, we will focus on this elemental architecture.

If the hinged bar and the middle slider are rigid and the side flappers only deform in bending, the total potential energy function of the Figure 2 bistable element,

$$\Pi = \frac{1}{2}k_s u^2 + \frac{1}{2}k_b v^2 - Fu \quad (1)$$

$$u = L_b(\cos\theta_0 - \cos\theta), \qquad v = L_b(\sin\theta - \sin\theta_0) \quad (2)$$

Here, θ is an inclination angle of the hinged bars in a state of equilibrium of the element in response to the external load F. Also, u is horizontal displacement of the slider, and v is vertical displacement of the flappers. Parameter L_b is length of the rigid hinged bars; k_s is axial stiffness of the encapsulated spring; $k_b = 12EI(3L_1 + L_2)/L_1^3(3L_1 + 4L_2)$ is bending stiffness of the elastic flappers, and θ_0 is initial of angle of the hinged bars, prior to loading. Both springs, k_s and k_b are relaxed when $\theta = \theta_0$. The spring k_s can be removed from the design, if necessary, by introducing a mismatch of lengths or initial angles of the hinged bars, for a similar performance. The spring stiffness k_s then can be replaced with a relevant mismatch parameter, but we omit these details for clarity of the main approach.

The potential energy (1) can be rescaled with a factor $k_b L_b^2$ to write a *dimensionless potential* in terms of only four dimensionless parameters $\{\theta, f, k, \theta_0\}$:

$$U = U(\theta, f; k, \theta_0) = \frac{1}{2}kx^2 + \frac{1}{2}y^2 - fx \tag{3}$$

$$k = \frac{k_s}{k_b}, \quad f = \frac{F}{k_b L_b}, \quad x = \frac{u}{L_b} = \cos\theta_0 - \cos\theta, \quad y = \frac{v}{L_b} = \sin\theta - \sin\theta_0 \tag{4}$$

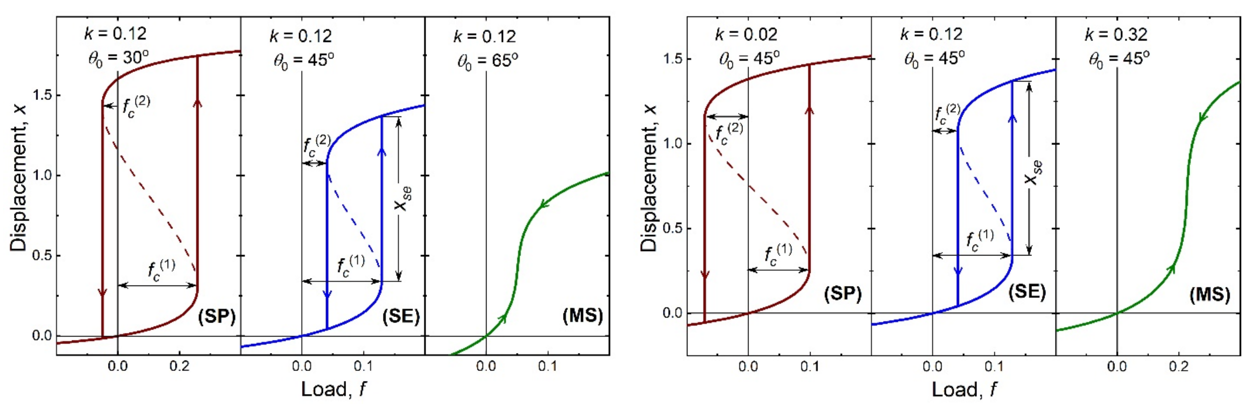

Fig.3: Three response types of the bistable axial bar element of Figure 2, realized at varying stiffness ratio k (left) and at varying initial angle θ_0 (right): bistable superplastic (SP), bistable superelastic (SE) and monostable (MS). The dash lines represent unstable equilibrium solutions.

Thus, there are two independent *design parameters* that can influence mechanical response qualitatively: (i) the ratio (k) of axial stiffness of the encapsulated spring and bending stiffness of the elastic flappers, and (ii) the initial of angle (θ_0) of the hinged bars prior to loading. The dimensionless axial force f is the *control parameter*, and inclination angle θ is the sole *state parameter* that fully describes a resultant state of equilibrium in the element.

3. **Response Curves & Bifurcations Diagrams: Properties of the Solution Space**

Analysis of response behavior of this and similar nonlinear systems is based on the first derivatives of the total potential energy with respect to the response parameters. The *equilibrium set*, written as an implicit function,

$$\Phi_e(\theta, f; k, \theta_0) = \frac{\partial U}{\partial \theta} = (1-k)\cos\theta + k\cos\theta_0 - \cot\theta\sin\theta_0 - f = 0 \tag{5}$$

contains all equilibrium responses θ of the model (3) for a given external load f and a particular set of design parameters $\{k, \theta_0\}$.

Solving for θ versus f from the condition (5) can be performed numerically, for example, using the methods outlined in [19-20,34,65], followed by calculation of the corresponding equilibrium displacement x by equation (4). The model (3) can demonstrate only three qualitatively different responses, $x(f)$, depending on the design parameters $\{k, \theta_0\}$, whose examples are shown in Figure 3: The highly nonlinear but *monostable* response is the first type. The bistable hysteretic response reversible to the initial configuration upon load removal, called *superelastic bistability*, is the second type. And the third type is the nonreversible hysteresis requiring load reversal for returning to the original configuration; that is called *superplastic bistability* [11,19-20,34]. Note that in the bistable responses, two different states of the structure exist, each with its own equilibrium angle for the same load. In more complex cases, the two states may demonstrate also different stiffnesses [11,19-20], in addition to different equilibrium angles or displacements.

Solving for θ versus the stiffness ratio k from the condition (5), at fixed f and θ_0, gives a bifurcation diagram whose example is given in Figure 4. This diagram shows how, with increase of k, the unstable solution and one of the stable solutions collide and annihilate each other at a saddle-node bifurcation point, when the value k becomes critically high, $k = k_c = 0.162$.

Similarly, solving for θ versus the initial angle θ_0 at a fixed load gives another diagram with a bifurcation point at $\theta_{0c} = 53.2^{\mathrm{o}}$, see Figure 4.

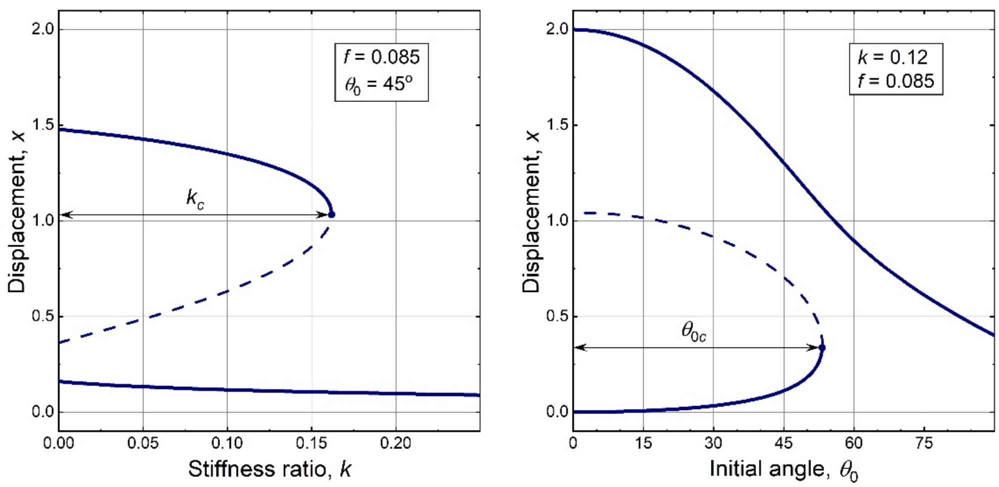

Fig.4: Examples of bifurcation diagrams for the bistable unit cell of Figure 2.

Interestingly, the bistable response curves in Figure 3 may also be viewed, alternatively, as bifurcation diagrams with two connected saddle-node bifurcations, where each of the bifurcations is associated with load-induced destabilization of the structure and transition between its two equilibrium states. Thus, critical values of the external load at the onset of destabilization are important characteristics of the bistable structure that need to be addressed in design.

The response curves and bifurcation diagrams of Figures 3-4 clearly shows that variance of the system parameters $\{k, \theta_0\}$ may lead to a desired bistable response, as in principle. However, two important design questions cannot be answered by analysis of the equilibrium set alone: (a) How do the system parameters $\{k, \theta_0\}$ influence values of the critical forces (f_c) at the onset of state transition of the structure, and (b) what is the allowable range of the design parameters $\{k, \theta_0\}$, so that structural response is still of a desired type from Figure 3? Addressing the *critical force magnitude and response type, as design objectives* require higher order analyses of the potential (3). These analyses lead to crafting stability and phase diagrams of the system discussed in Sections 4-5.

4. Stability Diagrams: Critical Loads as Design Objective

One important design objective is prediction of the critical forces (f_c), see Figure 3, based on the system parameters $\{k, \theta_0\}$. Critical values of control parameters are generally associated with the onset of destabilization and transition between different equilibrium states of multistable structures. The terms "snapping" is often used in relation to such transitions in simpler bistable structures [11-12,19].

A multistable system is destabilized at an inflection point of the potential (3) within the equilibrium set (5). Inflection points are generally found from the condition $\det H = 0$ with the Hessian matrix (H) of second order derivatives of a total potential energy function [19-20,34,66] with respect to state parameters of the system. When there is only one independent state parameter, as the angle θ in (3), we simply have the condition,

$$\frac{\partial^2 U}{\partial \theta^2} = (k-1)\sin\theta + \csc^2\theta \sin\theta_0 = 0 \qquad (6)$$

To be a physical bifurcation point, as in Figure 3-4 examples, an inflection point must also belong to the equilibrium set. Therefore, the two conditions (5-6) must hold simultaneously, i.e., $U'_\theta = U''_{\theta\theta} = 0$. This allows to eliminate the behavior variable (θ) from consideration and write a single equation that represents the so-called *bifurcation set* (or *critical set*), the locus of all bifurcation points of the system,

$$\Phi_b(f_c; k, \theta_0) = \frac{(f_c - k\cos\theta_0)^2}{\left(k-1+(1-k)^{1/3}\,\sin^{2/3}\theta_0\right)^2} + \frac{\sin^{2/3}\theta_0}{(1-k)^{2/3}} - 1 = 0 \qquad (7)$$

Here, f_c replaces f, because every bifurcation point corresponds to a certain critical force, as can be seen from Figures 3-4. Strictly speaking, k and θ_0 in (7) are also critical values of the system parameters, as we noted them k_c and θ_{0c} on the bifurcation diagrams of Figure 4. Thus, the implicit function (7) provides a practically important relationship between the critical forces $\{f_c\}$ and design parameters $\{k, \theta_0\}$ of the Figure 2 bistable structure. For more complex cases, two conditions of the type (5-6) can always be solved numerically to determine relationships between design parameters and critical values of control parameters; see [19-20,34,65] for some examples.

It is insightful to make 2D contour plots of the implicit function (7). Since it represents a 3D surface, one of the design parameters can be made fixed, and the other one is plotted versus the critical force f_c. Choosing the same set of design parameters as in Figure 3-4 plots, we obtain the diagrams of Figure 5. These are *stability diagrams* of the Figure 2 bistable structure. They allow determining, graphically, values of the design parameters $\{k, \theta_0\}$ that enable realization of certain desired critical loads.

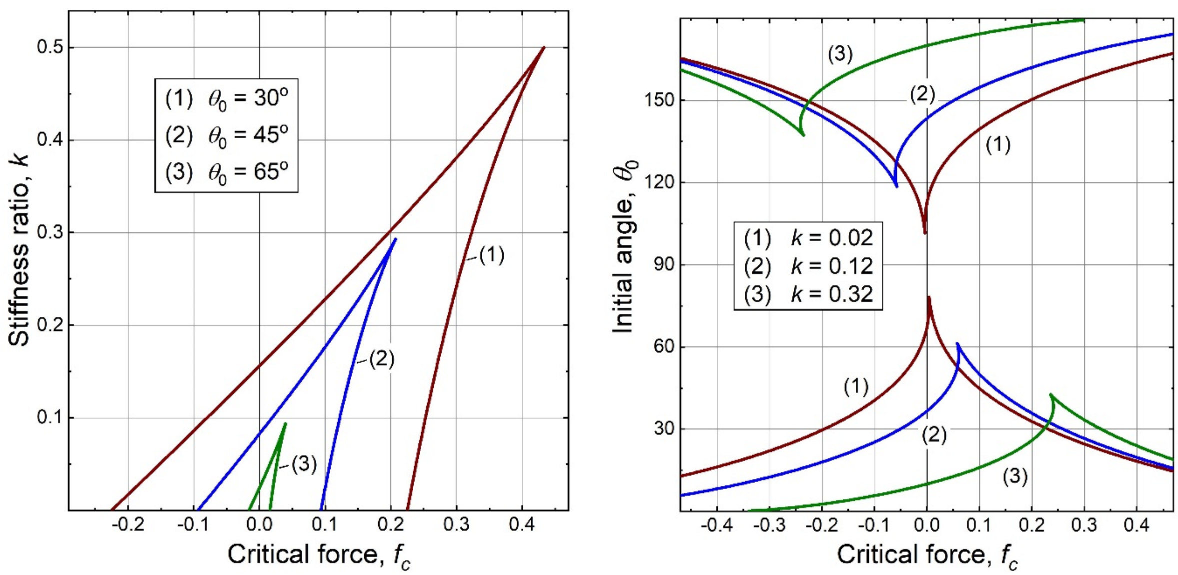

Fig.5: Stability diagrams of the bistable unit cell of Figure 2.

5. **Phase Diagram: Response Type as Design Objective**

The final stroke of brush in the basic analysis of bistable structures is the creation of its phase diagram. This will show all possible responses of the system, depending on its design parameters only. This requires elimination of both, state and control parameters from the consideration, and therefore calls for additional conditions to complement (5) and (6) in the analysis.

Condition 1 (*onset of superplasticity*): First, we note that with a decrease of k or theta θ_0, the response curves begin to intersect the axis $f = 0$. Therefore, the bifurcation set (7) contains a practically interesting subset (section), where one of the critical forces is zero:

$$\Gamma_E(k, \theta_0) = \Phi_b(0; k, \theta_0) = 0 \tag{8}$$

The plane curve $\Gamma_E = 0$ divides the design space $\{k, \theta_0\}$ into two parts. On the side of it, all responses are superplastic, see Figure 3, and on the other side, all responses are either superelastic or monostable.

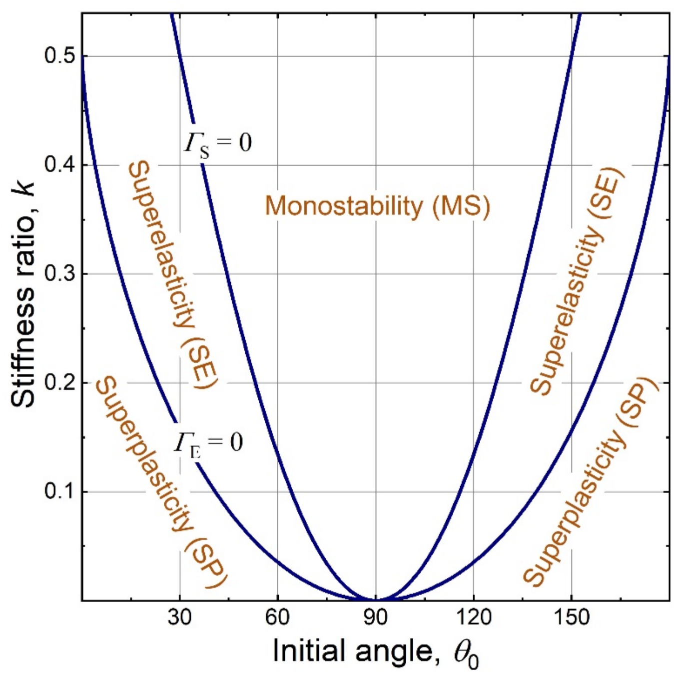

Fig.6: Phase diagram of the Figure 2 bistable element. The curves $\Gamma_E = 0$ and $\Gamma_S = 0$ are defined by the equations (8) and (10).

Condition 2 (*onset of bistability*): Second, we note from Figure 3 that with an increase of k or theta θ_0, the mechanical hysteresis may narrow to a single inflection point on the response curve, and then disappear entirely. Thus, condition for an inflection point on the response curve [11,19],

$$\frac{\partial^3 U}{\partial \theta^3} = (k-1)\cos\theta - 2\cot\theta\csc^2\theta\sin\theta_0 = 0 \tag{9}$$

must to be solved simultaneously with (5) and (6) to eliminate θ and f, leading to

$$\Gamma_S(k, \theta_0) = 1 - k - \sin\theta_0 = 0 \tag{10}$$

The plane curve $\Gamma_S = 0$ divides the design space $\{k, \theta_0\}$ into two regions. In the first region, all responses bistable (superelastic or superplastic), and in the second region, all responses are monostable.

A combined contour plot of the curves $\Gamma_E = 0$ and $\Gamma_S = 0$ by equations (8,10) gives, finally, the phase diagram of the Figure 2 bistable axial bar element, which is presented in Figure 6.

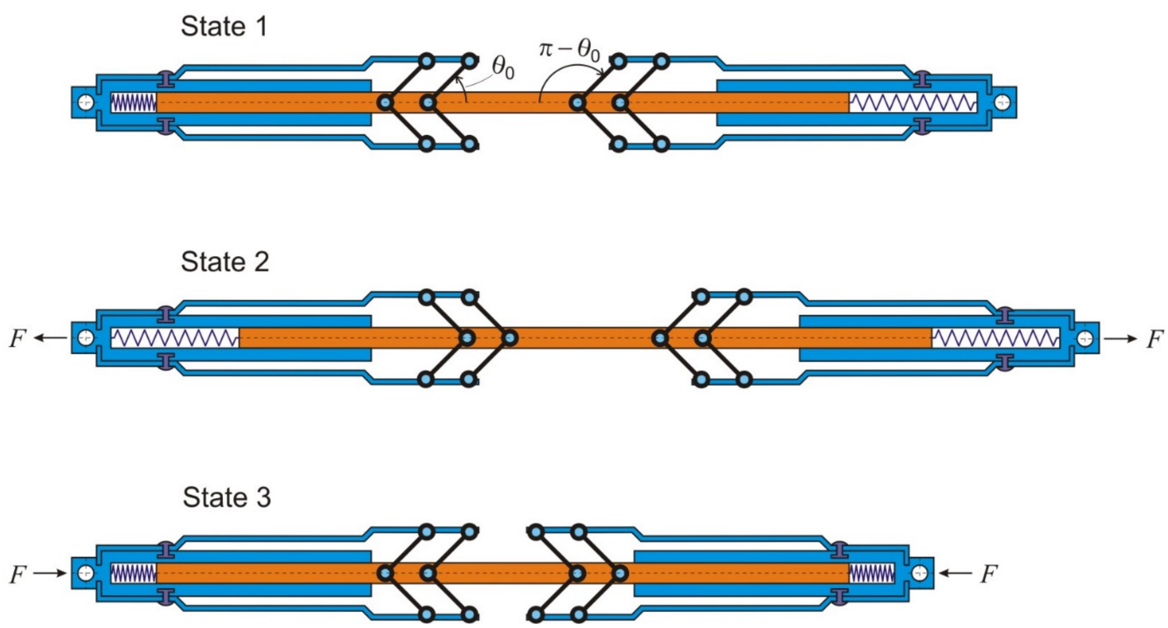

Fig.7: Composite bar structure, metabrace, comprised of two bistable elements of Figure 2 type, where initial angles of the hinged bars at zero load are θ_0 and $\pi - \theta_0$, respectively. Other design parameters are identical in two elements and the total structure potential, equation (11), is still defined by two design parameters $\{k, \theta_0\}$. All springs and elastic flappers are relaxed at zero load in the State 1.

6. A Tristable Bar: Two Antisymmetric Elements Combined

Comprehensive understanding of a base bistable element, as one of Figure 2 discussed above, enables design and property prediction of more complex structures comprised of several bistable cells. It is interesting to consider a pair of antisymmetric elements, with all identical properties (k, L_b), except for the initial hinged bars angle, being θ_0 in the first and $\pi - \theta_0$ in the second element. It is practical to arrange these elements in a single bar structure shown in Figure 7, where the elements are positioned face-to-face to share one slider. The slider is not loaded externally, and therefore, its displacement is an *internal* state parameter of the structure.

The total potential energy of such a structure can be written, based on (3),

$$U_S(\theta_1, \theta_2, f; k, \theta_0) = \frac{1}{2}k(x_1^2 + x_2^2) + \frac{1}{2}(y_1^2 + y_2^2) - f(x_1 + x_2) \tag{11}$$

$$x_1 = \cos\theta_0 - \cos\theta_1, \qquad y_1 = \sin\theta_1 - \sin\theta_0 \tag{12}$$

$$x_2 = \cos(\pi - \theta_0) - \cos\theta_2, \quad y_2 = \sin\theta_2 - \sin(\pi - \theta_0) \tag{13}$$

where θ_1 and θ_2 are inclination angles of the hinged bars in two elements in a loaded state.

It is interesting to see (a) what is the overall response of this structure to a varying axial load, and (b) if the theoretical analysis of Sections 2-5 can predict basic features of that response. Here, the most interesting features are values of the critical forces at the onset of snapping. For this purpose, we applied a numerical energy minimization technique to the potential (11) with $k = 0.12$ and different loads f, gradually varied in a closed cycle. Solutions from previous steps served as trial solutions for a next value of the load. The resultant response showed an interesting, *symmetric* double-hysteresis shape shown in Figure 8. This symmetry makes the structure practical for seismic applications where both, tensile and compressive loads should be anticipated equally. The *critical forces* are exactly those as for the unit cells of Figure 2, where $\theta_0 = 45^{\circ}$ in one cell, and $\theta_0 = 135^{\circ}$ in another cell. For the first cell, the critical forces are positive, representing a superelasticity in tension. For the second element, they are negative, standing for a superelasticity in compression. We also note the area of two hysteresis loops is the total work of external forces dissipated by the structure. This energy can be directly linked to a seismic efficiency, or another engineering measure of damping efficiency of this axial element in structural or mechanical engineering applications.

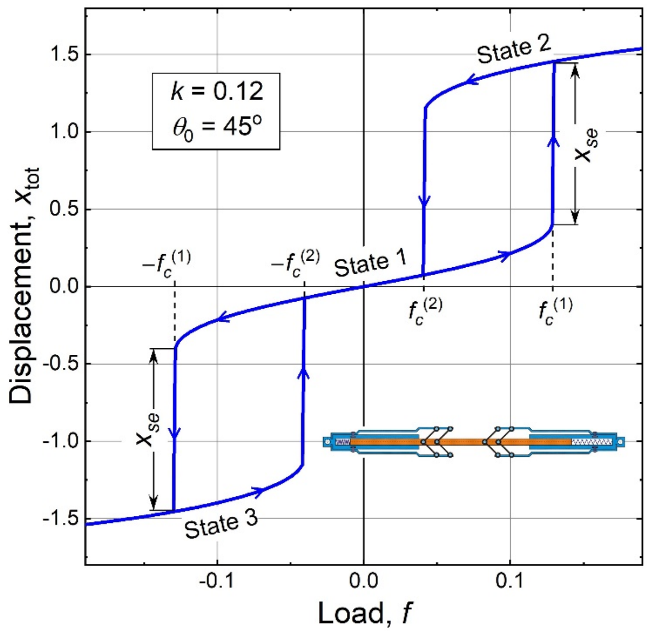

Fig.8: Sample tristable response (superelastic type) of Figure 7 metabrace at $k = 0.12$ and $\theta_0 = 45°$. Here, k and f are given in equation (4), and $x_{\text{tot}} = x_1 + x_2$, where x_1 and x_2 are from equations (12-13).

There are other important features of these structure that makes it well suitable for various structural applications. In addition to the total axial elongation, the structure also has an *internal* degree of freedom, the slider displacement. Kinetic energy of the external load can be efficiently dissipated on this degree of freedom with little viscous damping, and potentially, with *less acceleration* at the external degree of freedom, or at the end points of the brace. If M and m are masses of the base (blue) and slider (orange) parts of the metabraces in Figures 2 and 7, then maximal acceleration and velocity at both end points of the tristable metabrace will be approximately M/m times lower than those at the right end of the bistable metabrace in periodical axial load cycles.

Another practical significance if this tristable structure is a relative simplicity of its systematic stability analysis. In below, we explain a shortcut analysis approach that is made possible with the results obtained earlier for the Figure 2 bistable unit cell structure.

Involvement of additional internal degree of freedom in multistable systems generally leads to instabilities of an interactive types, or coincident instabilities, where a state transition is described by an abrupt change of values of two or more state parameters (total elongation and slider displacement in Figure 7 structure). Such a state transition is better described by a more general term "switching" [18-20], rather than "snapping". Stability analysis of coincident instabilities is generally more involved, although the overall approach described in Sections 2-5 is still valid. Based, on the potential (11), the *equilibrium set* is now defined by two simultaneous conditions,

$$\frac{\partial U_S}{\partial \theta_1} = \frac{\partial U_S}{\partial \theta_2} = 0 \tag{14}$$

and the *bifurcation set* points satisfy also a condition with the Hessian matrix determinant,

$$\det H = \begin{vmatrix} \frac{\partial^2 U_S}{\partial \theta_1^2} & \frac{\partial^2 U_S}{\partial \theta_1 \partial \theta_2} \\ \frac{\partial^2 U_S}{\partial \theta_2 \partial \theta_1} & \frac{\partial^2 U_S}{\partial \theta_2^2} \end{vmatrix} = 0 \tag{15}$$

These equations would represent a direct analysis approach of the Figure 7 tristable metabrace. However, we would like point out on a *shortcut approach*, taking into account the *series connection* of the two constitutive bistable elements of this structure. In this case, the potential U_S of equation (11), is additive:

$$U_S(\theta_1, \theta_2, f; k, \theta_0) = U(\theta_1, f; k, \theta_0) + U(\theta_2, f; k, \pi - \theta_0) \tag{16}$$

where U is the original unit cell potential (3). Therefore, the conditions (14) and (15) simplify to

$$\frac{\partial U(\theta_1)}{\partial \theta_1} = \frac{\partial U(\theta_2)}{\partial \theta_2} = \frac{\partial^2 U(\theta_1)}{\partial \theta_1^2} \cdot \frac{\partial^2 U(\theta_2)}{\partial \theta_2^2} = 0 \tag{17}$$

Thus, every critical point of the sought birfucation set must satisfy either this group of conditions,

$$\frac{\partial U(\theta_1)}{\partial \theta_1} = \frac{\partial^2 U(\theta_1)}{\partial \theta_1^2} = 0 \tag{18}$$

or this group of conditions,

$$\frac{\partial U(\theta_2)}{\partial \theta_2} = \frac{\partial^2 U(\theta_2)}{\partial \theta_2^2} = 0 \tag{19}$$

The first group of conditions defines a bifurcation set $\Phi_b(f_c; k, \theta_0)$, as in equation (7), and the second group defines a bifurcation set, $\Phi_b(f_c; k, \pi - \theta_0)$, with the same implicit function Φ_b, as given in equation (7). Since it is sufficient that only one group of conditions holds, (18) or (19), the sought *bifurcation set* of the Figure 7 tristable structure is given simply by a product of the two functions Φ_b:

$$\Phi_b(f_c; k, \theta_0) \cdot \Phi_b(f_c; k, \pi - \theta_0) = 0 \tag{20}$$

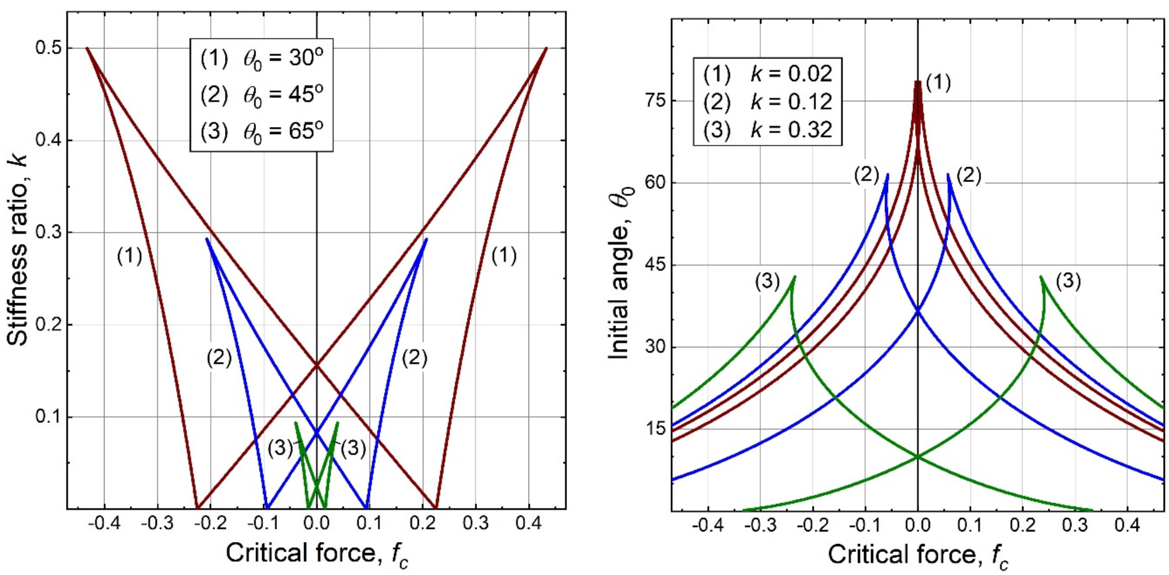

Fig.9: Stability diagrams of the Figure 7 tristable metabrace. Here, two symmetric pairs of critical forces exist for every superelastic or superplastic design $\{k, \theta_0\}$, consistent with the Figure 8 response type.

Plane sections of the set (20) at selected values of k or θ_0 serve as *stability diagrams* of the tristable metabrace, and their examples are shown in Figure 9. Here, interesting similarities with the Figure 5 diagrams can be seen. However, the present diagrams show four critical forces, rather than just two, for any combination of the parameters $\{k, \theta_0\}$ corresponding to a superelastic or superplastic behavior. A combination of the two bistable elements makes the stability diagrams symmetric with respect to a vertical axis, $f_c = 0$. This is a mathematical representation of the symmetry of mechanical properties of the tristable member with respect to tension and compression.

Due to the additive potential (16), *phase diagram* of the tristable bar is fully identical to that of the bistable base element, Figure 6, except that the angle θ_0 should be considered in the range from 0° to 90° only.

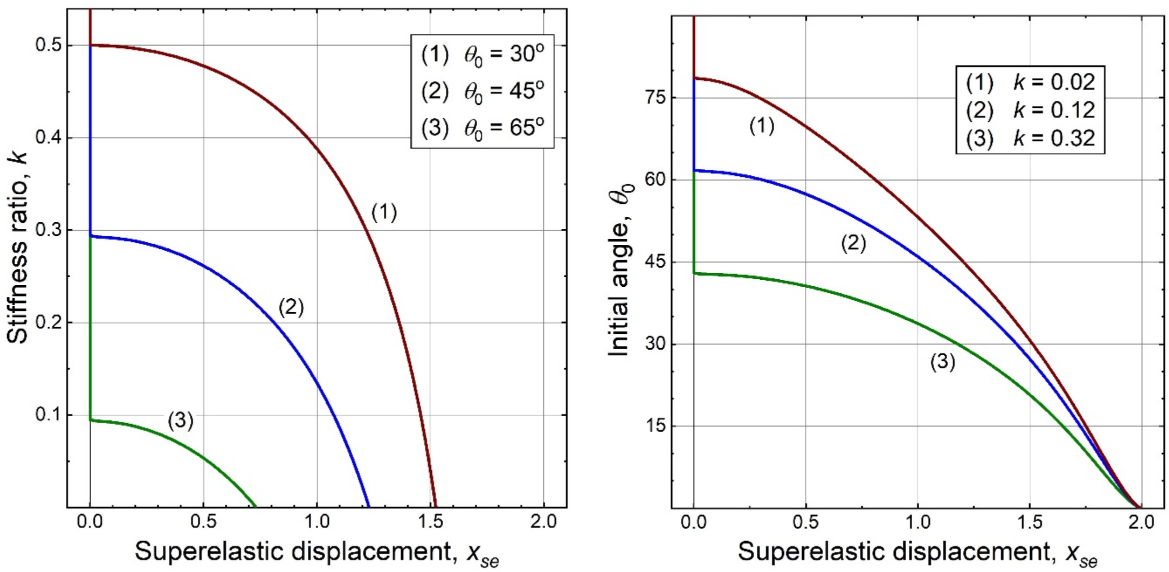

Fig.10: Variance of the superelastic displacement x_{se} in the bistable and tristable axial members of Figures 2 and 7 with their key design parameters $\{k, \theta_0\}$ defined by equation (4).

Finally, we note that the jump value, x_{se}, is an interesting characteristic of the structural responses in Figure 3 and Figure 8 plots. It determines a *superelastic elongation* and a *superelastic strain*, occurring due to a transition between the stable equilibrium states,

$$\delta_{se} = x_{se} L_b, \qquad \varepsilon_{se} = x_{se} \frac{L_b}{L} \tag{21}$$

where L is a relaxed length of the structure, and L_b is a hinged bars length, see Figure 2. Dependence of the x_{se} value on the key system parameters $\{k, \theta_0\}$ is important. Knowledge of this dependence may facilitate practical utility of the bistable and tristable metabraces discussed here. Since only one of the terms U in the symmetric additive potential (16) is exhibiting a superelastic transition at a critical axial load, the value x_{se} is *identical for the bistable and tristable structures* of Figures 2 and 7, and it can be determined from the original conditions (5) and (7). These conditions can provide some $\theta = \theta_c$ and f_c at every $\{k, \theta_0\}$. The angle θ_c is a critical angle of the hinged bars at the onset of a state transition, when the axial load is reaching the critical value f_c. The corresponding critical displacement, x_c, is given by the equation (4) at $\theta = \theta_c$. The superelastic response curve in Figure 3 indicates that another (stable) equilibrium displacement, x_e, exists for the same axial load $f = f_c$, belonging to the equilibrium set (5). The difference of these two displacements is then the sought superelastic displacement, $x_{se} = x_e - x_c$. Sample dependences of this interesting property of the bistable and tristable axial members on their key design parameters $\{k, \theta_0\}$ are shown in Figure 10.

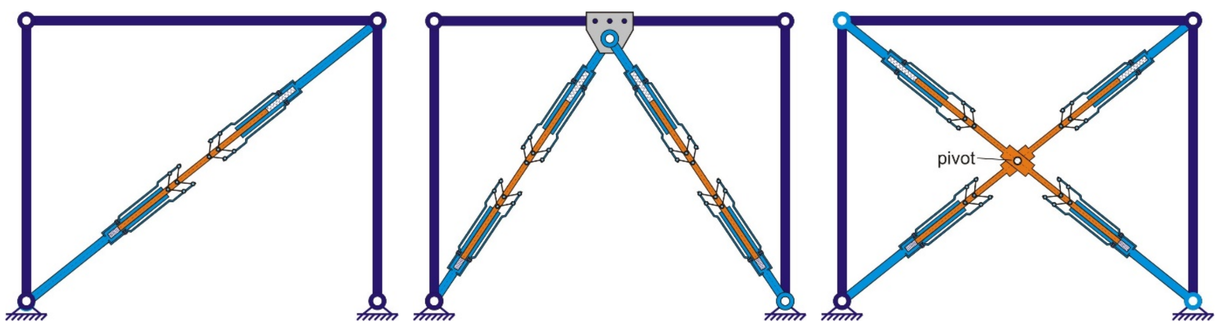

Fig.11: Examples of arrangement of multistable metabraces in the diagonal, chevron and X-type frames.

7. Remarks on Seismic Frame Design

As was mentioned in the introduction, concentrically braced steel frames, sacrifice their diagonal braces that could yield or buckle under excessive tension or compression in a seismic event, e.g. [4]. We suggest to replace diagonal braces of the concentric frames with the superelastic bi- and tristable metabraces of the types shown in Figures 2 and 7. Examples of the metabrace arrangement, in place of the former regular braces, are shown in Figure 11. One or two tristable elements could be used to provide a diagonal or chevron bracing, respectively. The X-bracing can be achieved with two tristable braces pivoted at their middle points on the sliders. This could also be viewed as an arrangement of two pairs of antisymmetric bistable elements, compare drawings in Figures 2, 7 and 11.

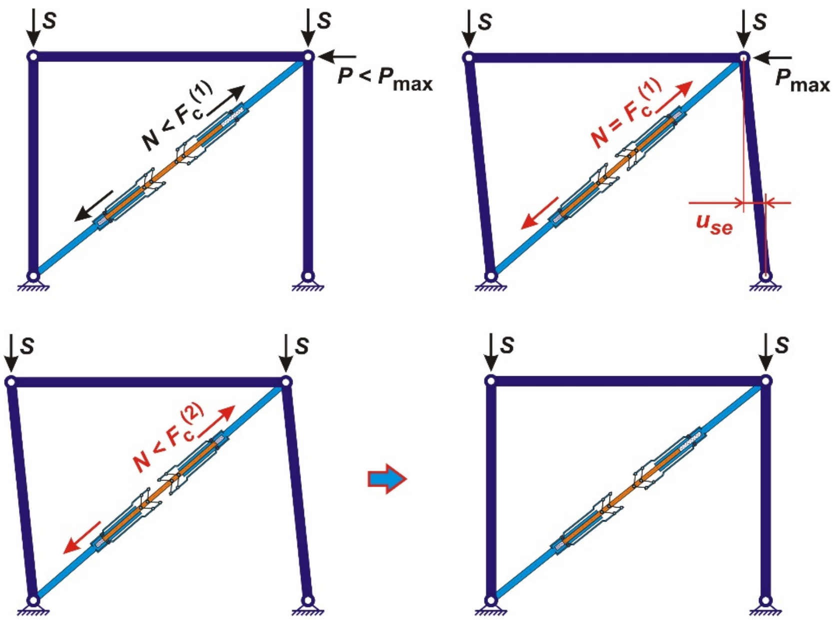

Fig.12: An illustration of the approach for critical forces (F_c) determination, based on the overall frame geometry and allowed superelastic displacement (u_{se}).

The nonlinear structural system analysis of Sections 2-6 can provide the *original dimensional parameters* $\{k_s, k_b, \theta_0, L_b, L\}$, as in Figures 2 and 7, and equations (1-4), for the metabrace fabrication. Various *procedures* will serve the purpose, for example, one could follow these steps: (a) The value L is selected as a relaxed total length of the metabrace to fit a nondeformed frame geometry, see Figure 11. (b) The initial angle θ_0 is selected referring to Fig.6 phase diagram, for which a desired (superelastic) response can be achieved for a reasonable stiffness ratio k. (c) An approach inspired by the capacity design method [66] is used to determine required critical forces and a superelastic displacement: The usual braces, replaced by the metabraces, would normally be expected to fail at a certain threshold intensity of the lateral load acting on the entire frame. An axial force in such a brace can be calculated at the onset of anticipated failure of the frame. This force then can be taken as a forward switching critical force, $F_c^{(1)} = f_c^{(1)} k_b L_b,$ of the metabrace, see Figure 12 for an example. Given some typical post-event structural load and a new structural configuration based on an anticipated superelastic displacement in the frame, a reverse switching critical force, $F_c^{(2)} = f_c^{(2)} k_b L_b$, is also found from standard structural analysis. Here, $F_c^{(2)}$ must exceed the axial member force in an equivalent usual frame, whose geometry is identical to a new configuration of the building frame determined by the superelastic displacement, u_{se}, see Figure 12. A required superelastic displacement in the metabraces $\delta_{se} = x_{se} L_b$, corresponding to $u_{se},$ is calculated using kinematical relationships for a given frame type. (d) A ratio $f_c^{(1)}/f_c^{(2)}$ is calculated and used with θ_0 in the Figure 9 stability diagrams to determine a stiffness ratio k, and a value $f_c^{(1)}$ corresponding to the combination $\{k, \theta_0\}$ is also recorded. (e) A value x_{se} is determined from Figure 10 type analysis using $\{k, \theta_0\}$, and then, the length $L_b = \delta_{se}/x_{se}$ is found using δ_{se} determined earlier. (f) The flapper's bending stiffness, $k_b = F_c^{(1)}/f_c^{(1)} L_b$, and the spring stiffness, $k_s = k_b k$, are calculated finally.

8. Conclusions

Approaches to systematic analysis of essentially nonlinear structures with bistabilities, controlled buckling and snapping behavior have received much attention recently in the context of mechanical metamaterials design. Mechanical bistability is defined as availability of two stable equilibrium configurations in a structure in response to the same loading conditions. A bistable element is generally a highly efficient damper, performing well even at very slow forcing frequencies. In this paper, we discussed and illustrated application of basic tools of this analysis to the macroscopic systems relevant to civil and mechanical engineering applications. Such systems are comprised of only several bistable elements, as contrasts to multistable mechanical metamaterial.

For a systematic discussion, inspired by the works [11,19-20,34,65], we divided all the relevant physical quantities into three groups: design, control (loads) and response (deformation) parameters. All interesting nonlinear properties of a single bistable axial, a two-force element, have been mapped out in the form of response curves, bifurcation, stability and phase diagrams.

Response curves show sample responses of the systems to external stimuli at given systems designs; bifurcation diagrams are plots of responses versus design parameters at given control parameters; stability diagrams link values of critical loads that induce state transitions with design parameters; and phase diagrams map all possible types of mechanical responses in terms of only design parameters of the system.

Three qualitatively different types of responses have been seen for a single (bistable) element: nonlinear monostability, superelastic bistability and superplastic bistability, as reflected on its phase diagram. Following a systematic analysis of the bistable element, we considered a combination of two elements with antisymmetric properties and demonstrated a robust *tristable* performance of the resultant structure in tension-compression loading cycles. The tristability has been shown to offer an overall response that is symmetric for tension and compression, which makes it interesting for large-scale structural applications and earthquake engineering. While buckling in conventional structural systems is an unwanted instability or failure, elastic buckling behavior of tristable brace element can be realized as an advantage to increase energy dissipation capacity and reduce stresses. Stability analysis of the trisatble element is made simple on the basis of the bistable element analysis. In particular, the tristable bifurcation set is shown to be a union of two bistable bifurcation sets with antisymmetric properties. Thus, comprehensive analysis of basic bistable mechanical elements, advocated here, paves the road toward property prediction and design of more complex multistable structures of a practical value.

While the superelastic behavior is probably most interesting in practice, the superplastic regimes (SP) with a negative reverse switching force might also be considered in the future for metaframes requiring simple post-event recovery treatment. A rate-dependent damping behavior can also be interesting, when the external load frequency reaches a significant fraction of the structural first mode frequency. The telescopic snapper design discussed here will then allow for an efficient control of structural damping, as desired, by manipulating both friction and a rate of air escape from the structure interior.

Acknowledgements

The authors are thankful to Prof. Oren Lavan of Technion for useful comments and discussions.

References

[1] Lui Z, Zhang X, Mao Y, Zhu Y, Yang Z, Chan C, Sheng P. Locally resonant sonic materials. *Science*, *289*, 1734–1736, 2000.

[2] Cummer SA, Christensen J, Alu A. Controlling sound with acoustic metamaterials. *Nature Review Materials*, *1*, 16001, 2016.

[3] Fang N, Xi DJ, Xu JY, Ambrati M, Sprituravanich W, Sun C, Zhang X. Ultrasonic Metamaterials with Negative Modulus. *Nature Materials*, 5, 452, 2006.

[4] Wang YZ, Li FM, Huang WH, Jiang X, Wang YS, Kishimoto, K. Wave band gaps in two-dimensional piezoelectric/piezomagnetic phononic crystals. *International Journal of Solids and Structures*, *45*, 4203–4210, 2008.

[5] Hussein MI, Leamy MJ, Ruzzene M. Dynamics of phononic materials and structures: historical origins, recent progress, and future outlook. *Applied Mechanics Review* 66 (4), 040802, 2014.

[6] Mousavi SH, Khanikaev AB, Wang Z. Topologically protected elastic waves in phononic metamaterials. *Nature Communications*, 6, 8682, 2015.

[7] Kolpakov AG. Determination of the average characteristics of elastic frameworks. *Journal of Applied Mathematics and Mechanics*, 49, 6, 739-745, 1985

[8] Lakes RS. Foam structures with a negative Poisson's ratio. *Science*, *235*, 1038–1040, 1987.

[9] Lakes RS. Negative Poisson's ratio materials. *Science*, *238*, 551, 1987.

[10] Stavroulakis GE. Auxetic behaviour: Appearance and engineering applications. *Physica Status Solidi B*, *242* (3),710–720, 2005.

[11] Danso, LA, Karpov, EG. Cusp singularity-based bistability criterion for geometrically nonlinear structures. *Extreme Mechanics Letters*, 13, 135-140, 2016.

[12] Rafsanjani A, Akbarzadeh A, Pasini D. Snapping Mechanical Metamaterials under Tension. *Advanced Materials*, 27, 39, 5931–5935, 2015.

[13] Silverberg JL, et al. Origami structures with a critical transition to bistability arising from hidden degrees of freedom. *Nature Materials, 14*, 389–393, 2015.

[14] Waitukaitis S, Menaut R, Chen BG-g, van Hecke M. Origami multistability: From single vertices to metasheets. *Physical Review Lett*ers, *114*, 055503, 2015.

[15] Nicolau ZG, Motter AE. Mechanical metamaterials with negative compressibility transitions. *Nature Materials*, *11*, 608, 2012.

[16] Nicolau ZG, Motter AE. Longitudinal inverted compressibility in super-strained metamaterials, *Journal Statistical Physics, 151*,1162, 2013.

[17] Imre AR. Metamaterials with negative compressibility – a novel concept with a long history. *Materials Science-Poland*, *32*, 126–129, 2014.

[18] Chen ML, Karpov EG. Bistability and thermal coupling in elastic metamaterials with negative compressibility. *Physical Review E*, *90*, 033201, 2014.

[19] Karpov EG, Danso LA, Klein JT. Negative Extensibility metamaterials: Occurrence and design space topology. *Physical Review E*, 96(2), 023002, 2017.

[20] Klein JT, Karpov EG. Negative extensibility metamaterials: phase diagram calculation, *Computational Mechanics*, 1–15, 2017.

[21] Karpov EG. Structural metamaterials with Saint-Venant edge reversal. *Acta Materialia,123*, 245-254, 2017.

[22] Danso LA, Karpov EG. Reprogramming static deformation patterns in mechanical metamaterials. *Materials*, 11, 2050, 2018.

[23] Karpov EG, Danso L A. Strain Energy Spectral Density and Information Content of Materials Deformation*. International Journal of Mechanical Sciences*, 148, 676-683, 2018.

[24] Karpov EG, Danso LA, Klein JT. Anomalous strain energy transformation pathways in mechanical metamaterials. *Proceedings of the Royal Society A*, 2019004, 2019.

[25] Dong L, Lakes R. Advanced damper with high stiffness and high hysteresis damping based on negative structural stiffness. *International Journal of Solids and Structures, 50*, 2416–2423, 2013.

[26] Zadpoor AA. Mechanical meta-materials. *Materials Horizons*, *3*, 371–381, 2016.

[27] Bertoldi K, Vitelli V, Christensen J, van Hecke M. Flexible Mechanical Metamaterials. *Nature Review Materials, 2*(11), p. 17066, 2017.

[28] Yu XL, Zhou J, Liang HY, Jiang ZY, Wu LL. Mechanical metamaterials associated with stiffness, rigidity and compressibility: A brief review. *Progress Materials Science*, *94*, 114–173, 2018.

[29] Lakes R, Cellular solids with tunable positive or negative thermal expansion of unbounded magnitude. *Applied Physics Letters*, 90 (22), 221905, 2007.

[30] Grima JN, Farrugia PS, Gatt R, Zammit V. A system with adjustable positive or negative thermal expansion. *Proceedings of the Royal Society A*, 463 (2082), 1585–1596, 2007.

[31] Wang Q, Jackson JA, Ge Q, Hopkins, JB, Spadaccini, CM, Fang NX. Lightweight mechanical metamaterials with tunable negative thermal expansion. *Physical Review Letters*, 117 (17), 175901, 2016.

[32] Wu L, Li B, Zhou J. Isotropic negative thermal expansion metamaterials, *ACS Applied Materials and Interfaces*, 8 (27), 17721–17727, 2016.

[33] Ai L, Gao XL. Metamaterials with negative Poisson's ratio and non-positive thermal expansion. *Composite Structures*, 162, 70–84, 2017.

[34] Klein JT, Karpov EG. Bistability in thermomechanical metamaterials structured as three-dimensional composite tetrahedra. *Extreme Mechanics Letters*, 29,100459, 2019.

[35] Khomeriki R, Lepri S, Ruffo S. Nonlinear supratransmission and bistability in the Fermi-Pasta-Ulam model, *Physical Review E* 70, 066626, 2004.

[36] Gammaitoni L, Neri I, Vocca H. Nonlinear oscillators for vibration energy harvesting, *Applied Physics Letters* 94(16), 164102, 2009.

[37] Stanton SC, McGehee CC, Mann BP. Nonlinear dynamics for broadband energy harvesting: investigation of a bistable piezoelectric inertial generator, *Physica D* 239(10), 640-653, 2010.

[38] Arrieta AF, Hagedorn P, Erturk A, Inman DJ. A piezoelectric bistable plate for nonlinear broadband energy harvesting, *Applied Physics Letters* 97(10), 104102, 2010.

[39] Karpov EG. Bistability, Autowaves and Dissipative Structures in Semiconductor Fibers with Anomalous Resistivity Properties. *Philosophical Magazine* 92(10), 1300–1316, 2012.

[40] Harne RL, Thota M, Wang KW. Concise and high-fidelity predictive criteria for maximizing performance and robustness of bistable energy harvesters, *Applied Physics Letters* 102(5), 053903, 2013.

[41] Wu Z, Harne RL, Wang KW. Energy harvester synthesis via coupled linear-bistable system with multi-stable dynamics, *ASME Journal of Applied Mechanics* 81(6), 061005, 2014.

[42] Lydon J, Theocharis G, Daraio C. Nonlinear resonances and energy transfer in finite granular chains, *Physical Review E* 91, 023208, 2015.

[43] Wu Z, Harne RL, Wang KW. Exploring a modular adaptive metastructure concept inspired by muscle's crossbridge, *Journal of Intelligent Material Systems and Structure*, 27(9), 1189-1202, 2016.

[44] Harne RL, Wang KW. *Harnessing Bistable Structural Dynamics - for Vibration Control, Energy Harvesting, and Sensing*, John Wiley and Sons, ISBN: 978-1-119-12804-5, 2017.

[45] Wu Z, Zheng Y, Wang KW. Metastable modular metastructures for on-demand reconfiguration of band structures and non-reciprocal wave propagation, *Physical Review E*, 97, 022209, 2018.

[46] Wu Z, Wang KW. On the wave propagation analysis and supratransmission prediction of a metastable modular metastructure for nonreciprocal energy transmission, *Journal of Sound & Vibration*, 458, 389-406, 2019.

[47] Taichiro T, Lignos D, Mitsumasa M, Ricles J, Love J. Damage to Steel Buildings Observed after the 2011 Tohoku-Oki Earthquake, *Earthquake Spectra* 29, 219, 2013.

[48] Chou, C., Chen, S.Y. Subassemblage tests and finite element analyses of sandwiched buckling-restrained braces, *Engineering Structures* 32(8):2108–2121, 2010.

[49] Zhao, J., Wu, B., Ou, J. A novel type of angle steel buckling-restrained brace: Cyclic behavior and failure mechanism, *Earthquake Engng. Struct. Dyn.* 40:1083–1102, 2011.

[50] Ma, N., Ou, J.P., Li, H. Experimental Study of Low-yield Strength Steel Buckling Restrained Brace, *Proceedings of 15 WCEE*, Lisbon, Portugal, 2012.

[51] Dusicka, P., Tinker, J. Global Restraint in Ultra-Lightweight Buckling-Restrained Braces. *J. Compos. Constr.* 17, 139-150, 2013.

[52] Eryasar, M. E., and Topkaya, C. An Experimental Study on Steel-Encased Buckling-Restrained Brace Hysteretic Dampers, *Earthquake Engng Struct. Dyn*. 39, 561–581, 2010.

[53] Shen, J., Seker, O., Sutchiewcharn, N., Akbas, B. Cyclic behavior of buckling-controlled braces. *Journal of Constructional Steel Research* 121, 110–125, 2016.

[54] Seker O, Akbas B, Seker PT, Faytarouni M, Shen J, Mahamid M. Three-Segment Steel Brace for Seismic Design of Concentrically Braced Frames, *Journal of Constructional Steel Research* 137, 211-227, 2017.

[55] Erochko J, Christopoulos C, Tremblay R. Design and Testing of an Enhanced-Elongation Telescoping Self-Centering Energy-Dissipative Brace, *Journal of Structural Engineering* 141(6), 04014163, 2015.

[56] Erochko J, Christopoulos C, Tremblay R. Design, Testing, and Detailed Component Modeling of a High-Capacity Self-Centering Energy-Dissipative Brace, *Journal of Structural Engineering* 141(8): 04014193, 2015.

[57] Xu LH, Fan XW, Li ZX. Development and experimental verification of a pre-pressed spring self-centering energy dissipation brace, *Engineering Structures* 127, 49–61, 2016.

[58] Issa AS, Alam MS. Experimental and numerical study on the seismic performance of a selfcentering bracing system using closed-loop dynamic (CLD) testing, *Engineering Structures* 195, 144–158, 2019.

[59] Xu L, Fan X, Li Z. Experimental behavior and analysis of self-centering steel brace with pre-pressed disc springs, *Journal of Constructional Steel Research* 139, 363–373, 2017.

[60] Xiea Q, Zhou Z, Meng SP. Experimental investigation of the hysteretic performance of self-centering buckling-restrained braces with friction fuses, *Engineering Structures* 203, 109865, 2020.

[61] Xie Q, Zhou Z, Huang JH, Zhu DP, Meng SP. Finite-Element Analysis of Dual-Tube Self-Centering Buckling-Restrained Braces with Composite Tendons, *J. Compos. Constr.* 21(3), 04016112, 2017.

[62] Xie Q, Zhou Z, Huang JH, Meng SP. Influence of tube length tolerance on seismic responses of multi-storey buildings with dual-tube self-centering buckling-restrained braces, *Engineering Structures* 116, 26–39, 2016.

[63] Hu S, Wang W, Qu B. Seismic evaluation of low-rise steel building frames with self-centering energy-absorbing rigid cores designed using a force-based approach, *Engineering Structures* 204, 110038, 2020.

[64] Xu LH, Fan XW, Li ZX. Cyclic behavior and failure mechanism of self-centering energy dissipation braces with pre-pressed combination disc springs, *Earthquake Engng Struct. Dyn.* 46, 1065-1080, 2017.

[65] Strogatz SH. Nonlinear Dynamics and Chaos. *Addison-Wesley Publishing Company*, 1994.

[66] Saunders PT. An Introduction to catastrophe theory. *Cambridge University Press*, 1980.